ORIGINAL ARTICLE

Planar radionuclide angiography with a dedicated cardiac SPECT camera

R. Glenn Wells, PhD, FCCPM,[a,b] Brian Marvin, BA, MRT(N), CNMT,[b] Gil Kovalski, PhD,[c] and Terrence D. Ruddy, MD, FRCPC, FACC[a,b]

Background. We compared a dedicated cardiac camera with a traditional system for left ventricular (LV) functional measurements using gated blood-pool imaging.

Methods. 24-frame gated planar images were obtained from 48 patients in an LAO orientation for 6M counts/view on a standard gamma camera. Immediately thereafter, 24-frame ECG-gated data were obtained for 8 minutes on a dedicated cardiac SPECT camera. The gated SPECT image volumes were iteratively reconstructed and then transferred offline. In-house software was used to reproject the images into a 24-frame gated planar format. Both the original and the reprojected gated planar datasets were analyzed using semiautomated software to determine ejection fraction (EF), ventricular volume (end diastolic volume, EDV), peak ejection rate (PER), and peak filling rate (PFR).

Results. The difference in EF values averaged 0.4% ± 4.4%. The correlation in EF was $r \geq 0.94$ ($P < .01$) with a linear regression slope of 0.98. Correlation of the EDV was $r \geq 0.86$ ($P < .01$), but the volumes from the dedicated cardiac camera were smaller (linear regression slope was 0.6). Correlation of PFR and PER were $r = 0.91$ and $r \geq 0.83$, respectively ($P < .01$ for both).

Conclusions. Reprojection of 24-frame gated blood-pool SPECT images is an effective means of obtaining LV functional measurements with a dedicated cardiac SPECT camera using standard 2D-planar analysis tools. (J Nucl Cardiol 2013;20:358–66.)

Key Words: Radionuclide angiography · left ventricular function · ejection fraction · dedicated cardiac SPECT

INTRODUCTION

Dedicated cardiac SPECT cameras have recently been introduced, which offer many advantages over traditional SPECT systems.[1-3] The new cameras use multiple detectors that are focused on the heart, and the design provides a greatly increased sensitivity. Some of the systems also use cadmium-zinc-telluride (CZT) detectors that have greatly improved energy resolution.[1,4,5] The application of these systems has been directed at myocardial perfusion imaging (MPI), and the new cameras have been shown to perform similar to traditional designs, but with acquisition duration being reduced to as low as 2 minutes.[1,6-13]

Nuclear imaging is frequently used to measure ventricular function with planar gated blood-pool imaging or radionuclide angiography (RNA). The American College of Cardiology, the American Heart Association, and the American Society of Nuclear Cardiology (ASNC) guidelines[14] indicate that RNA has a class I indication for the assessment of left ventricular (LV) function following infarction, in the context of chronic coronary artery disease and heart failure, and following heart transplantation. It also has a class I indication for initial and serial assessment of LV function in patients receiving cardiotoxic drugs, those with valvular heart disease, or those with congenital heart disease. The ASNC recommendations include a number of parameters that can be drawn from the RNA exam including ejection fraction (EF), ventricular volumes, wall motion, peak ejection rate (PER) and peak filling rate (PFR).[14]

A limitation of the new dedicated cardiac SPECT systems is their inability to acquire a dynamic planar image as is typically done for an RNA exam. However, with multiple detector heads and stationary or near-stationary cameras, the temporal resolution of the cameras for 3D imaging is much better than with traditional systems. Traditional SPECT camera acquisitions are typically limited to 8 or 16 gates over the cardiac cycle, and this limits the accuracy of measures like EF, PER, and PFR. Consequently, ASNC recommends 24-32 gates for planar studies that measure these parameters.[14] The high sensitivity and temporal resolution of the new dedicated cameras make it practical to acquire 24-frame gated SPECT studies. However, in our center and many others, functional analysis of RNA studies is done on dynamic 2D datasets, and the requisite software to evaluate the 3D dynamic images may not be available. This problem can be overcome by collapsing the gated 3D data via summation along a line through the volume such as the left-anterior oblique (LAO) direction normally used for planar imaging. The summation re-creates the 2D dynamic planar dataset that has been commonly used for analysis.

Our objective for this study is to evaluate RNA measurements of 2D planar studies created through reprojection of SPECT data acquired on a dedicated cardiac camera and compare them to those acquired with gated planar measurements from a traditional gamma camera. This approach allows for comparison against an established method of analysis and provides information on the backward compatibility of results from the new hardware to those from dynamic planar studies acquired previously on traditional cameras.

METHODS

Patients

Patients were recruited from the population undergoing a clinically indicated gated blood-pool study in our clinic between January and August 2010 and between March 2011 and January 2012. All patients signed informed consent, which was approved by the University of Ottawa Heart Institute Research Ethics Board. A total of 52 patients agreed to participate. Of these, four cases were excluded. In one case, there was very poor uptake in the blood-pool and considerable activity in the stomach indicating a failure of the radiolabeling. In one case, we were unable to obtain a consistent gating signal resulting in very low counts within the timing acceptance window for both cameras. In one case, the patient had considerable breast attenuation on the LAO view and had had a Mustard correction of a transposition of the great arteries, resulting in very poor definition of what was anatomically the LV. The fourth case was excluded because of technical difficulties in retrieving the traditional camera's gated planar

data from our database. The exclusion of these four cases left a total of 48 studies for comparison. Patients' demographics are given in Table 1.

Gated Blood-Pool Imaging with a Traditional NaI Camera

All the patients underwent a standard equilibrium blood-pool imaging study using ^{99m}Tc-labeled red blood cells in accordance with the recommendations proposed by ASNC.[14] Labeling was performed using the modified in-vivo/in-vitro method of injecting stannous chloride into the patient, withdrawing blood from the patient, and labeling the blood ex-vivo with 1,200 MBq ^{99m}Tc-pertechnetate, and reinjecting the blood back into the patient. LAO images were acquired with 24-frame ECG-gating and recorded in a 64×64 array with a timing acceptance window of $\pm15\%$. The total number of counts acquired in the timing acceptance window was 5.7 ± 0.5 million counts. Data were obtained using standard NaI-based gamma cameras: either a Cardial (GE Healthcare), pixel size of 3.44 mm, or an Infinia (GE Healthcare), pixel-size of 4.42 mm.

Dedicated Cardiac Camera Imaging

Immediately following the acquisition on the standard gamma camera, an additional set of data was acquired using a dedicated cardiac camera with cadmium-zinc-telluride (CZT)-based detectors (Discovery NM 530c, GE Healthcare). Projection data were acquired for 8 minutes, and ECG-gated to 24-frames with an acceptance window of $\pm10\%$. The total number of counts acquired in the timing acceptance window was 16.5 ± 6.5 million counts. The projection data were then reconstructed with vendor-supplied iterative reconstruction into a 24-frame gated blood-pool SPECT image volume. The voxel size was 4 mm^3, and the reconstruction did not include compensation for either attenuation or scatter. The image volume was exported, and further processing was performed off-line using the in-house software. The SPECT images were reprojected at an LAO angle (the projection angle was adjusted to that which visually corresponded to the angle acquired with the traditional camera). The reprojection assumed an ideal parallel hole collimation and did not include attenuation, scatter, or distance-dependent collimator resolution. The resulting 24-frame gated planar image was re-imported back into our clinical systems for standard blood-pool analysis.

Blood-Pool Analysis

The 24-frame gated planar studies from both the traditional camera and the dedicated cardiac camera were transferred to a Hermes processing workstation and analyzed using the FUGA program (Hermes Medical Systems).[15] By means of this software, the LV is detected automatically within a user-defined region but can manually be adjusted as needed. The FUGA software uses a cycle-dependent background correction for which the background ROI is not only automatically positioned but can also be adjusted manually.

Table 1. Patient demographics (n = 48 patients)

Gender	Age (years)	Height (m)	Weight (kg)
79% M	54.3 ± 11.7 [20-84]	1.73 ± 0.09 [1.54-1.93]	83.9 ± 18.0 [50-123]

Mean ± standard deviations are given as well the range of values.

Processing was done independently by two experienced operators. The values for EF, estimated cardiac end diastolic volume (EDV), PFR, and PER were compared. The EF was calculated based on the difference in counts between the ROI values at end-diastole and end-systole divided by the background-corrected counts at end-diastole. The EDV was calculated based on the pixel size and the ratio of the maximum counts in the ROI to the total counts.[16] The PFR and PER were calculated from the slopes of the time-activity curves and expressed in units of end-diastolic volume per second. Mean values of parameters were compared using a paired student's *t*-test, and the correlation was assessed with a Pearson's correlation coefficient and Bland-Altman analysis.

Further study of the estimated volume of the ventricle was done using an anthropomorphic cardiac-torso phantom (Data-Spectrum). The ventricle of the phantom was filled with 85 MBq (2.3 mCi) of 99mTc-pertechnetate. The phantom was placed on the traditional gamma camera (Infinia, GE Healthcare), and acquisitions were acquired (1) over 90° (right-anterio oblique to left posterior oblique) with the two head positioned 90° apart; (2) over 180° with the two heads positioned 180° apart; and (3) as a static view with the phantom and camera positioned to obtain a short-axis view. The SPECT data were reconstructed with filtered backprojection (FBP) and ordered-subset expectation maximization without correction and with combinations of attenuation correction (AC), dual-energy window scatter correction (SC), and resolution recovery (RR). RR was performed using the Evolution software package (GE Healthcare). Post-reconstruction filtering was applied to all images and selected to match the one used for our NM 530c camera reconstructions. The filter was a 3D 7th-order Butterworth filter with a cut-off frequency of 0.4 cycles/cm, which was similar to the manufacturer's default. Data were also obtained with the same phantom positioned in the NM 530c camera. The NM 530c data were reconstructed with and without attenuation correction, with 200 iterations (I200), and without the noise-suppression prior (No-OSL). Reconstructed volumes were summed along the long-axis of the heart to create planar images, and volumes were estimated from these planar images by the same method as was used in this study.[16] Volumes were also estimated based on counting those voxels in the image with counts greater than a fixed percent of the maximum. The threshold was chosen such that the traditional camera reconstructed with AC and SC reproduced the true volume (60 mL).

RESULTS

Illustrative images acquired with the traditional NaI-based planar gamma camera and a reprojected planar image from the CZT-based dedicated cardiac SPECT camera are given in Figure 1, along with their corresponding time-activity curves. With respect to the measured EF, the correlation coefficient between the two operators was $r = 0.96$ (mean difference = 2.4% ± 3.8%, $P < .01$) and $r = 0.97$ (mean difference = 1.6% ± 3.9%, $P < .01$) for the dedicated and traditional camera data, respectively. The correlations were both significant ($P < .01$), but there was a small but statistically significant difference in the EF values of the two operators, and thus the results for a single observer are presented in Figure 2. However, for the two operators, the correlation between the dedicated and traditional camera EF was not significantly different ($P = .58$) and averaged $r = 0.94$ ($P < .01$). The mean difference between the two cameras was not significantly different for the two observers ($P = .16$) and averaged 0.4% ± 4.0% ($P = .48$; 1.96 SD = 7.8%). The Bland-Altman plots show no trends as a function of mean EF. The plots also indicate that there were a few outliers with larger differences between the dedicated and traditional camera studies; however, 71% of the studies had a difference of ≤3%, while 94% of the studies had a difference of ≤6%.

With respect to the measured EDV, the correlation coefficients for the two operators were $r = 0.98$ ($P < .01$; mean difference = 9 ± 14 mL, $P < .01$) and $r = 0.98$ ($P < .01$; mean difference = 13 ± 18 mL, $P < .01$) for the dedicated and traditional camera data, respectively. Though their EDV values are statistically different, the results of the camera comparison for the two observers are very consistent. The correlation between the dedicated and traditional camera EDV was not significantly different for the two operators ($P = .69$); it averaged $r = 0.87$ ($P < .01$) (Figure 3). However, linear regression on the EDV scatter plot (Figure 3A) gives a slope of 1.42, suggesting that the traditional camera volumes are consistently more than 40% larger than those seen with the dedicated system. The mean difference between the two cameras was not significantly different for the two observers ($P = .22$) and averaged 78 ± 53 mL ($P < .01$; 1.96 SD = 103 mL). The Bland-Altman plot (Figure 3B) shows a correlation between the mean EDV and the EDV difference between the two cameras ($r = 0.57$, $P < .01$). Linear regression on the Bland-Altman plots shows that the difference is approximately
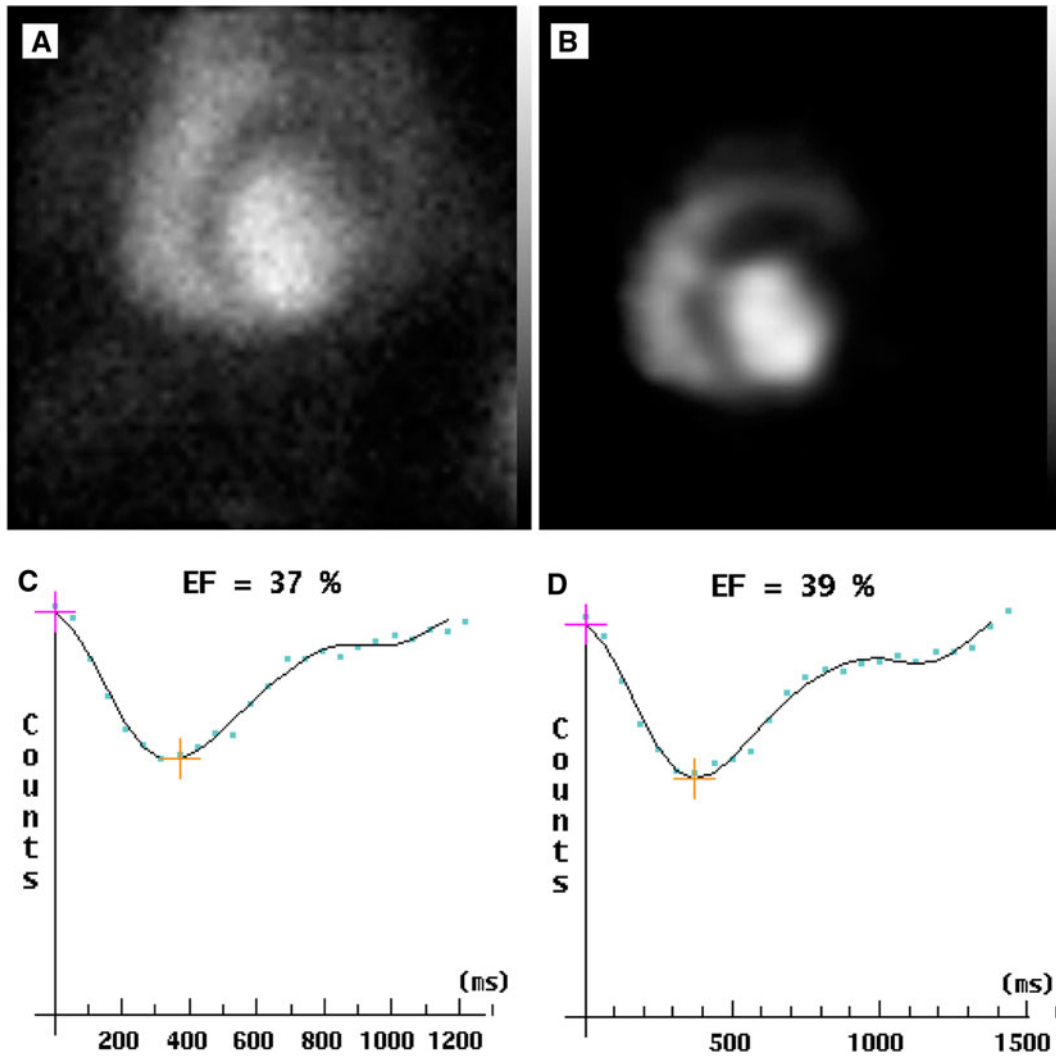
Figure 1. Example images from a traditional planar NaI camera (**A**) and the reprojection of a SPECT blood-pool volume acquired with a dedicated cardiac CZT camera (**B**). The corresponding EF are shown below in **C** and **D**.

equal to 40% of the mean value (Figure 3C). The results of the volume estimates from the phantom experiment are given in Table 2.

With respect to the measured PFR, the correlation coefficients for the two operators were $r = 0.97$ (mean difference $= 0.03 \pm 0.18$ ED/second, $P = .32$) and $r = 0.96$ (mean difference $= 0.02 \pm 0.22$ ED/second, $P = .62$) for the dedicated and traditional camera data, respectively. As the correlations are significant ($P < .01$ for both) with $r \geq 0.96$ and there are no significant differences in the mean values, the PFR data from the two observers were averaged together. The correlation between the dedicated and traditional camera PFR was $r = 0.91$ ($P < .01$) (Figure 4). Linear regression gives a slope of 0.82 with an intercept of 0.26 ED/second. The mean difference between the two cameras was

0.03 ± 0.32 ED/second ($P = .46$; 1.96 SD $= 0.63$ ED/second). The Bland-Altman plot shows no trends as a function of mean PFR. 71% of the studies had a difference of ≤ 0.3 ED/second, while 94% of the studies had a difference of ≤ 0.6 ED/second.

With respect to the measured PER, the correlation coefficient for the two operators was $r = 0.95$ (mean difference $= 0.07 \pm 0.19$ ED/second, $P = .02$) and $r = 0.96$ (mean difference $= 0.05 \pm 0.21$ ED/second, $P = .09$) for the dedicated and traditional camera data, respectively. Although their PER values for the dedicated camera were statistically different, the results of the camera comparison for the two observers were consistent. The correlation between the dedicated and traditional camera PER was not significantly different for the two observers ($P = .69$) and averaged $r = 0.85$
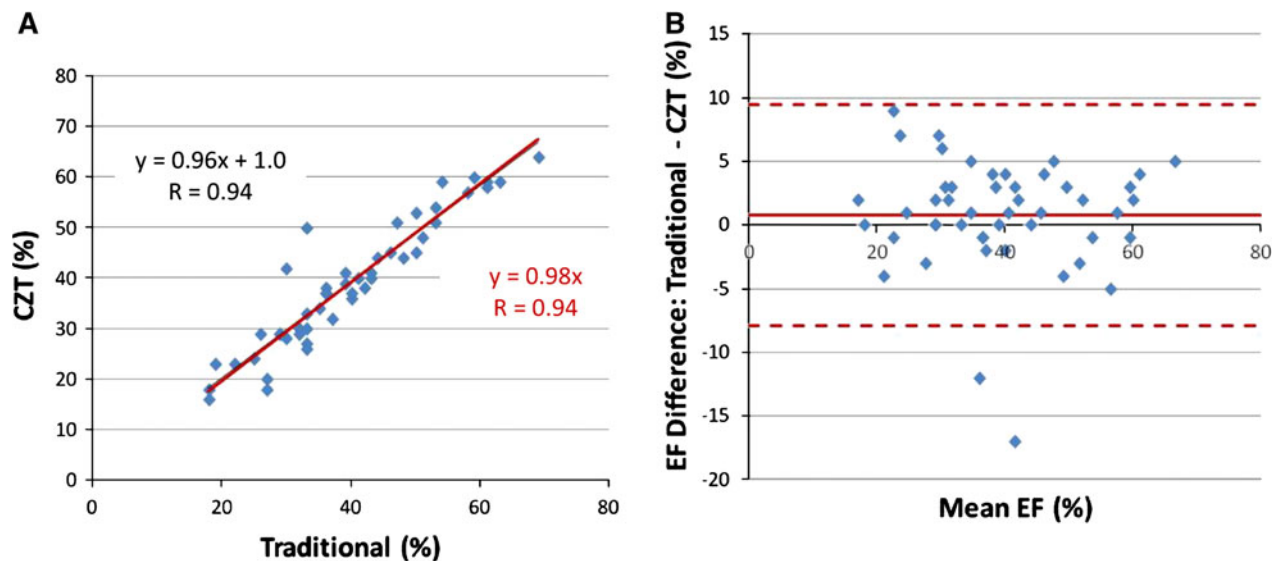
Figure 2. Comparison of EF between traditional and dedicated cardiac cameras for one of the observers. A scatter plot comparing the traditional and CZT cameras is at *left* (**A**), and the Bland-Altman analysis is at *right* (**B**). The mean difference is indicated by the *solid red line*, and the 1.96 SD 95% confidence levels are indicated by the *dashed red lines*.

for the two observers (Figure 5). The mean difference between the two cameras was not significantly different between the two operators ($P = .68$) and averaged 0.11 ± 0.37 ED/second ($P = .05$; 1.96 SD = 0.70 ED/second). The Bland-Altman plot shows a correlation between the PER difference and the mean PER value of $r = 0.25$, but this was not significant ($P = .09$). 67% of the studies had a difference of ≤ 0.36 ED/second, while 90% of the studies had a difference of ≤ 0.54 ED/second.

DISCUSSION

EF values are very well correlated with very little shift in the absolute value. The differences between observers for the dedicated system and the differences between the dedicated and traditional system for both observers were less than the 4% uncertainty found for measuring EF with RNA.[15] Therefore, EF measurements from the reprojected dedicated cardiac camera data could be compared with earlier measurements on traditional systems. EDV, PFR, and PER also correlated very well with correlation coefficients of $r \geq 0.83$, but the actual values for EDV and PER were significantly different. A reduction in ventricular volumes estimated with the dedicated cardiac camera was also seen in earlier studies assessing myocardial perfusion imaging[7] and may be associated with the exact algorithms used to perform the calculations. In this study, the EDV was estimated based on the ratio of maximum to total counts within the ROI. One of the problems with this approach is that the shape of

the ventricle is assumed to be spherical, and this is not always an accurate approximation of the true ventricle's shape. The algorithm also does not consider the impact of variable attenuation on the measured counts or other effects such as scatter, distance-dependent collimator resolution, and post-filtering. As shown in Table 2, the phantom study reproduced a similar difference in volume estimates as was seen in the clinical data. With the phantom experiments, we found attenuation correction (without SC) produced a 5% difference in volumes with the traditional camera data and <2% change with the NM530c camera. The application of SC introduced a large error in volumes, larger than those seen with the NM530c system. The use of RR also introduced changes in the estimated volumes. Finally, we observed little impact from using the noise-suppression prior in the NM530c reconstruction, but a gain in accuracy by increasing the number of iterations from 40 (without AC) or 60 (with AC) to 200. However, increasing the number of iterations used increases the required reconstruction time proportionately and given the strong correlation in the EDV values, rescaling of the reconstructed volumes presents a more practical solution. We also note that a more direct measurement of the ventricle volume using a threshold provided more consistent results for all of the reconstructions. The NM530c reconstructions done without AC and 40 iterations produced volumes that were 18% lower but with attenuation correction, the error was only 6%, and increasing the number of iterations to 200 further reduced the error to 1%. The greater consistency and improved concordance of the traditional and NM530c results with
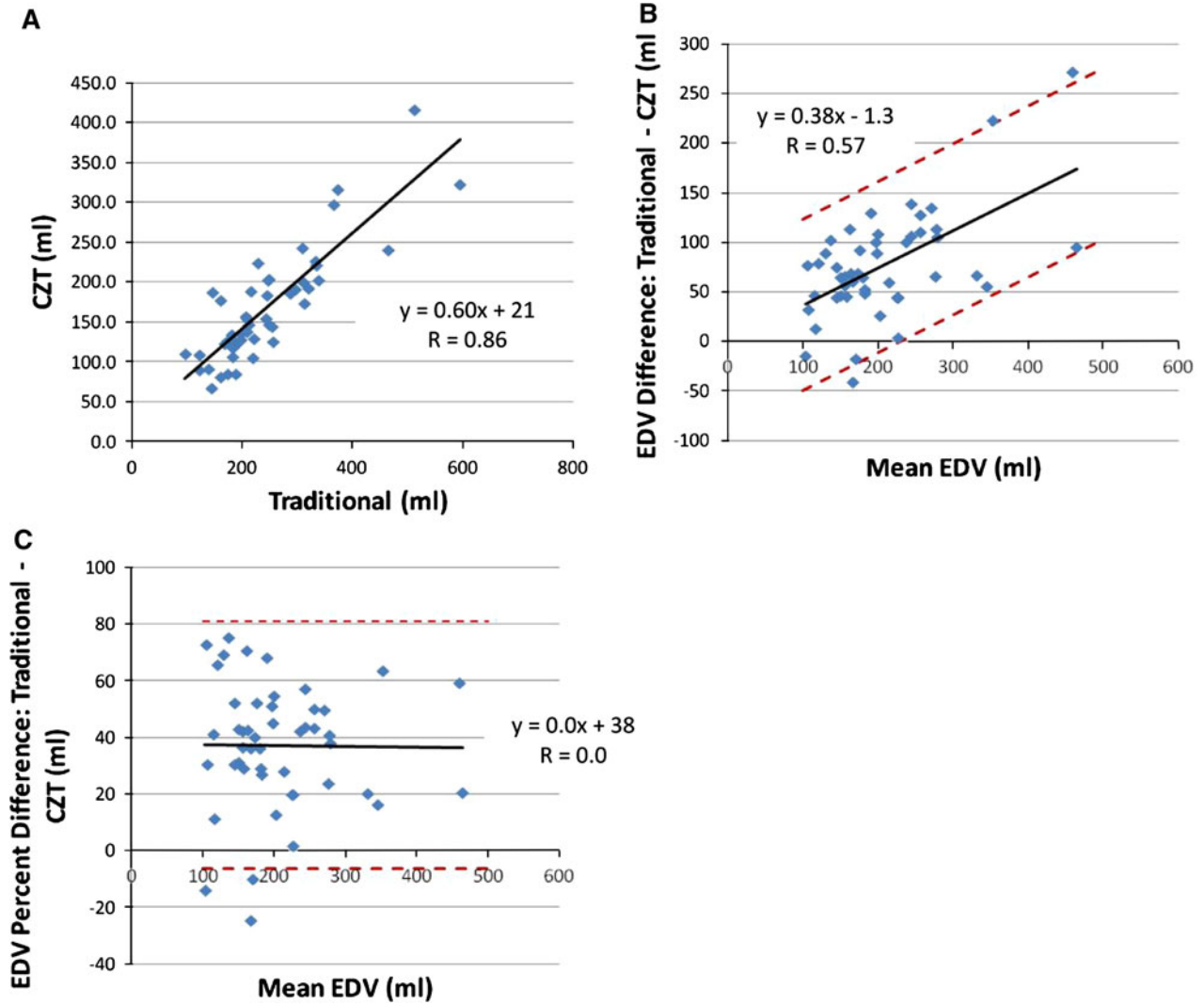
Figure 3. Comparison of EDV between traditional and dedicated cardiac cameras for one of the observers. A scatter plot comparing the traditional and CZT cameras is at *top left* (**A**), the Bland-Altman analysis is at *top right* (**B**) and a plot of the percent difference against the mean is at *bottom left* (**C**). Linear fits to the differences are given by the *solid black lines* and the 1.96 SD 95% confidence levels are indicated by the *dashed red lines*. There is a correlation ($r = 0.6$) between the differences and the mean values in the Bland-Altman plot (see text) corresponding to a 40% reduction in volume for the CZT-based camera.

the thresholding approach demonstrate some of the limitations inherent in the estimation of volumes from planar data.

Our results suggest that for EDV and PER measures, care should be taken in comparing values obtained from the two different camera systems. New normal ranges will need to be established to allow for comparison with earlier studies done on traditional systems.

The correlation between the two operators for the dedicated camera was very similar to that from the traditional system suggesting that interoperator variability is similar for the two cameras. The values obtained

for the measured parameters showed small but statistically significant differences for the two observers, but these differences were similar for both cameras. This suggests that the differences were caused by differing preferences for the placement of the background region and the designation of the ventricular wall.

Care needs to be taken in choosing an appropriate background region. The dedicated system used in this study has a spherical field-of-view that is greatly reduced in size with variable sensitivity throughout because of the use of pinhole collimation. In addition, attenuation is known to influence the dedicated system's images

Table 2. Ventricle volume evaluation using a Cardiac-Torso phantom

Acquisition	Reconstruction	Volume estimated from planar image (mL)	Percent difference (%)	Volume estimated by threshold (mL)	Percent difference (%)
Planar	n/a	60.9	1.5	n/a	n/a
	SC	38.1	−36.5	n/a	n/a
Infinia-180	FBP	61.0	1.7	62.4	4.0
	OSEM	60.3	0.5	59.7	−0.5
	ACSC	42.7	−28.8	60.0	0.0
	AC	57.3	−4.5	61.8	3.0
	RR	56.4	−6.0	61.4	2.3
	ACSCRR	52.6	−12.3	70.8	18.0
Infinia-90	FBP	59.5	−0.8	57.9	−3.5
	OSEM	54.6	−9.0	55.5	−7.5
	ACSC	40.8	−32.0	60.0	0.0
NM 530c	MLEM	43.5	−27.5	49.5	−17.5
	AC	43.1	−28.2	56.6	−5.7
	I200	48.1	−19.8	55.9	−6.8
	I200-AC	47.0	−21.7	60.7	1.2
	No OSL	43.2	−28.0	47.4	−21.0
	No OSL-AC	43.2	−28.0	56.6	−5.7

The true volume is 60 mL.
FBP, Filtered backprojection; *OSEM*, ordered subset expectation maximization; *MLEM*, maximum likelihood expectation maximization; *AC*, attenuation correction; *SC*, dual-energy-window scatter correction; *RR*, resolution recovery; *I200*, 200 iterations of the reconstruction algorithm; *OSL*, noise suppression prior; *Infinia-180*, the traditional-camera acquisition with the heads at 180 to each other; *Infinia-90*, the traditional-camera acquisition with the heads at 90 to each other.
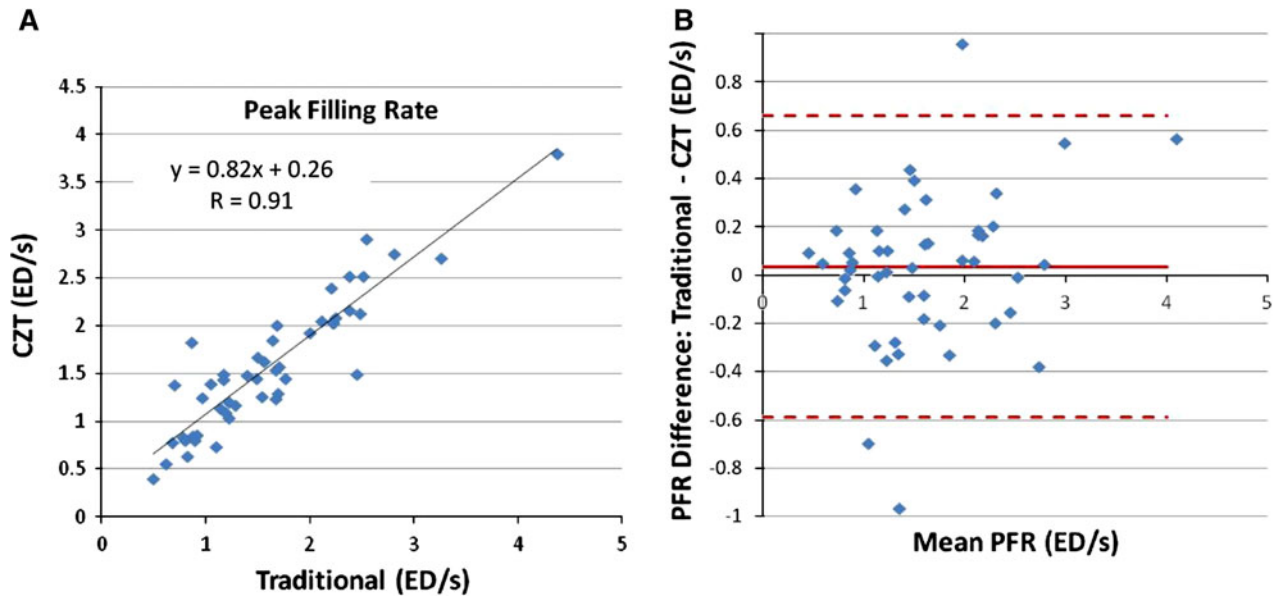

Figure 4. Comparison of PFR between traditional and dedicated cardiac cameras averaged over the two observers. A scatter plot comparing the traditional and CZT cameras is at *top* (**A**) and the Bland-Altman analysis is at *bottom* (**B**). The mean difference is indicated by the *solid red line* and the 1.96 SD 95% confidence levels are indicated by the *dashed red lines*.
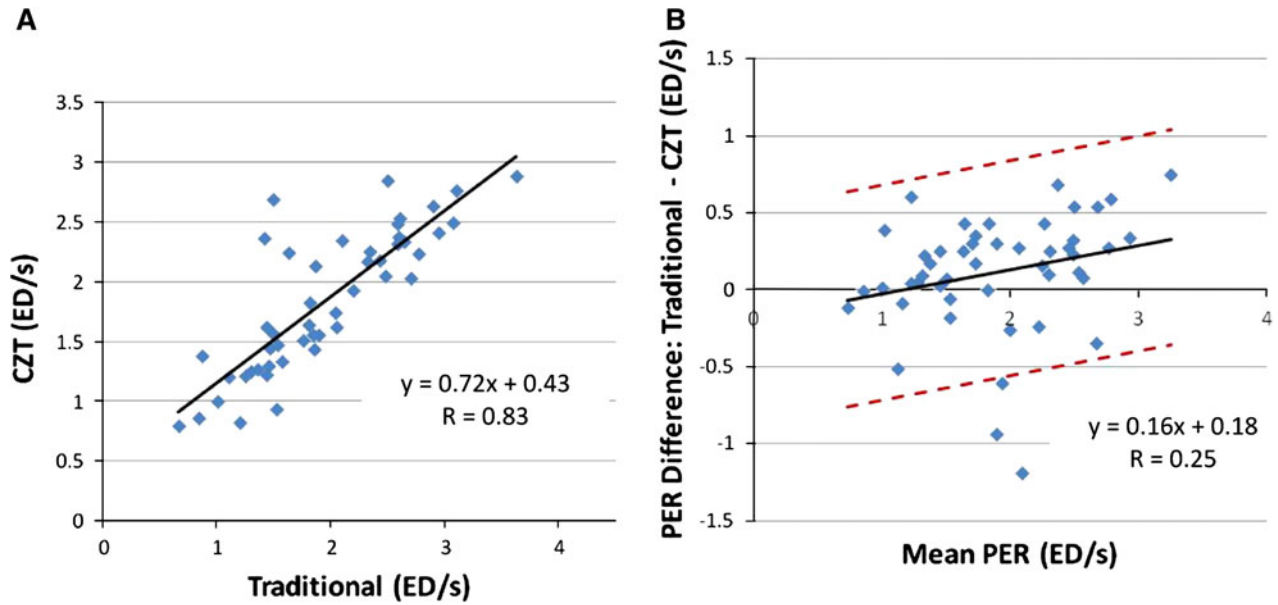
Figure 5. Comparison of PER between traditional and dedicated cardiac cameras for one of the observers. A scatter plot comparing the traditional and CZT cameras is at *left* (**A**), and the Bland-Altman analysis is at *right* (**B**). A linear fit to the data is indicated by the *solid black line*, and the 1.96 SD 95% confidence levels are indicated by the *dashed red lines*. The Bland-Altman plot shows a weak correlation of the PER difference with the mean PER.

differently than that in standard systems.[7] These factors influence the amount of background contributing to each portion of the reprojection, and a poor choice of the region used for background correction will significantly impact on the values obtained with the study.

The dedicated cardiac system has a small FOV of approximately 19-cm diameter[5] which may raise concerns over truncation of the images. None of the hearts in this study was truncated despite cardiac volumes being as large as 600 mL. Care should, nevertheless, be taken to ensure that the entire ventricle is centered in the FOV as truncation of the activity distribution can lead to artifacts at the edge of the FOV. The location of the FOV is fixed with respect to the camera head, and thus there are a small number of large patients for whom it is not possible to position them such that their heart is in the FOV. With this small subset of patients, imaging with this camera is not recommended.

The reprojected images from the dedicated system have lower spatial resolution than those obtained directly as planar images with a traditional system. Though this did not impair the correlation of EF and EDV, the effect on other types of evaluations such as wall motion or phase analysis still requires further investigation. An advantage of the SPECT-reprojection approach is that the angle of reprojection can be adjusted after acquisition, allowing optimization of the view that best separates the LV.

Software such as Quantitative Bloodpool SPECT (QBS—Cedars Sinai, Los Angeles, CA)[,17] and 4DM SPECT (Invia, Ann Arbor, MI)[18] are capable of measuring parameters directly from SPECT blood-pool studies. 3D evaluation avoids interference from background structures such as the atria and overlying tissues. SPECT blood-pool thus has the potential to improve the accuracy of the functional measurements.[19] However, a limitation of SPECT imaging with traditional cameras has been the difficulty in obtaining sufficient counts to support gating with large numbers of frames such as the 24 gates typically used with planar evaluation. The dedicated cameras with their increased sensitivity now offer the possibility of providing SPECT images with these frame rates. This has the potential to improve the accuracy. Evaluation of gated blood-pool SPECT imaging with the dedicated systems now capable of these high frame rates is a topic for further investigation.

The acquisition time for the CZT system was not optimized. Given the increased sensitivity, it should be possible to greatly reduce the total acquisition time for the study and/or reduce the injected activity and hence the patient radiation exposure. However, with the differences in methodology, 2D planar vs SPECT followed by reprojection, it is not immediately clear as to what should the optimal acquisition time for the dedicated camera be. Based on our study, 8 minutes is sufficient, but further study to determine if this time could be reduced without loss of accuracy is required.

A limitation of this study is the small number of patients studied. The small population limits the ability to detect small changes in the measured values. However, the patient sampling in our study is representative of the range of function typically seen with this diagnostic test and so reflects the clinical distribution.

CONCLUSION

This study found significant correlation between using a dedicated cardiac camera and a traditional approach for blood-pool gated imaging with $r \geq 0.94$ for EF and $r \geq 0.83$ for the other parameters measured. The value for EF matched well between the two systems, but the EDV and PER values were significantly different suggesting a need for the establishment of new normal limits for the dedicated camera. Reprojection of the gated dedicated cardiac SPECT image provides an effective means of creating traditional planar blood-pool datasets.

References

1. Slomka PJ, Patton JA, Berman DS, Germano G. Advances in technical aspects of myocardial perfusion SPECT imaging. J Nucl Cardiol 2009;16:255-76.
2. Garcia EV, Faber TL, Esteves FP. Cardiac dedicated ultrafast SPECT cameras: New designs and clinical implications. J Nucl Med 2011;52:210-7.
3. Schillaci O, Danieli R. Dedicated cardiac cameras: a new option for nuclear myocardial perfusion imaging. Eur J Nucl Med Mol Imaging 2010;37:1706-9.
4. Erlandsson K, Kacperski K, van Gramberg D, Hutton BF. Performance evaluation of D-SPECT: A novel SPECT system for nuclear cardiology. Phys Med Biol 2009;54:2635-49.
5. Bocher M, Blevis IM, Tsukerman L, Shrem Y, Kovalski G, Volokh L. A fast cardiac gamma camera with dynamic SPECT capabilities: Design, system validation and future potential. Eur J Nucl Med Mol Imaging 2010;37:1887-902.
6. Sharir T, Ben-Haim S, Merzon K, Prochorov V, Dickman D, Ben-Haim S, et al. High-speed myocardial perfusion imaging initial clinical comparison with conventional dual detector anger camera imaging. JACC Cardiovasc Imaging 2008;1:156-63.
7. Esteves FP, Raggi P, Folks RD, Keidar Z, Askew JW, Rispler S, et al. Novel solid-state-detector dedicated cardiac camera for fast myocardial perfusion imaging: Multicenter comparison with standard dual detector cameras. J Nucl Cardiol 2009;16:927-34.
8. Berman DS, Kang X, Tamarappoo B, Wolak A, Hayes SW, Nakazato R, et al. Stress thallium-201/rest technetium-99m Sequential dual isotope high-speed myocardial perfusion imaging. JACC Cardiovasc Imaging 2009;2:273-82.
9. Gambhir SS, Berman DS, Ziffer J, Nagler M, Sandler M, Patton J, et al. A novel high-sensitivity rapid-acquisition single-photon cardiac imaging camera. J Nucl Med 2009;50:635-43.
10. Buechel RR, Herzog BA, Husmann L, Burger IA, Pazhenkottil AP, Treyer V, et al. Ultrafast nuclear myocardial perfusion imaging on a new gamma camera with semiconductor detector technique: First clinical validation. Eur J Nucl Med Mol Imaging 2010;37:773-8.
11. Herzog BA, Buechel RR, Katz R, Brueckner M, Husmann L, Burger IA, et al. Nuclear myocardial perfusion imaging with a cadmium-zinc-telluride detector technique: Optimized protocol for scan time reduction. J Nucl Med 2010;51:46-51.
12. Sharir T, Slomka PJ, Hayes SW, DiCarli MF, Ziffer JA, Martin WH, et al. Multicenter trial of high-speed versus conventional single-photon emission computed tomography imaging: Quantitative results of myocardial perfusion and left ventricular function. J Am Coll Cardiol 2010;55:1965-74.
13. Ben-Haim S, Kacperski K, Hain S, Van Gramberg D, Hutton BF, Erlandsson K, et al. Simultaneous dual-radionuclide myocardial perfusion imaging with a solid-state dedicated cardiac camera. Eur J Nucl Med Mol Imaging 2010;37:1710-21.
14. Corbett JR, Akinboboye OO, Bacharach SL, Borer JS, Botvinick EH, DePuey EG, et al. Quality assurance committee of the american society of nuclear cardiology. Equilibrium radionuclide angiocardiography. J Nucl Cardiol 2006;13:e56-79.
15. De Bondt P, De Winter O, Vandenberghe S, Vandevijver F, Segers P, Bleukx A, et al. Accuracy of commercially available processing algorithms for planar radionuclide ventriculography using data for a dynamic left ventricular phantom. Nucl Med Commun 2004;25:1197-202.
16. Massardo T, Gal RA, Grenier RP, Schmidt DH, Port SC. Left ventricular volume calculation using a count-based ratio method applied to multigated radionuclide angiography. J Nucl Med 1990;31:450-6.
17. Daou D, Harel F, Helal BO, Fourme T, Colin P, Lebtahi R, et al. Electrocardiographically gated blood-pool SPECT and left ventricular function: Comparative value of 3 methods for ejection fraction and volume estimation. J Nucl Med 2001;42:1043-9.
18. Kritzman JN, Corbett JR, Ficaro EP. Comparison of diastolic function parameter estimates from planar and SPECT blood pool imaging. J Nucl Cardiol 2004;11:S7.
19. Daou D. SPECT radionuclide angiography: It is time for a consensus statement. Eur J Nucl Med Mol Imaging 2007;34:1729-34.